Weierstraß-Institut
für Angewandte Analysis und Stochastik

im Forschungsverbund Berlin e.V.

Preprint ISSN 0946 – 8633

Influence of anisotropic thermal conductivity in the apparatus insulation for sublimation growth of SiC: Numerical investigation of heat transfer

Jürgen Geiser[1], Olaf Klein[1] and Peter Philip[2]

submitted: 9th June 2005

[1] Weierstrass Institute
for Applied Analysis
and Stochastics
Mohrenstrasse 39
D-10117 Berlin
Germany
E-Mail: geiser@wias-berlin.de
klein@wias-berlin.de

[2] Institute for Mathematics
and its Applications (IMA)
University of Minnesota
400 Lind Hall
207 Church Street S.E.
Minneapolis, MN 55455-0436
USA
E-Mail: philip@ima.umn.edu

No. 1034
Berlin 2005

2000 *Mathematics Subject Classification.* 80A20 80M25 74S10 76R50 74E10 35J60 35J65 65Z05.

Key words and phrases. Numerical simulation. SiC single crystal. Physical vapor transport. Heat transfer. Anisotropic diffusion. Anisotropic thermal conductivity. Nonlinear elliptic PDE's.

2003 *Physics Abstract Classifications.* 02.60.Cb 81.10.Bk 44.05.+e 47.27.Te.

This work has been supported by the DFG Research Center Matheon – "Mathematics for key technologies" (FZT 86) in Berlin and by the Institute for Mathematics and its Applications (IMA) in Minneapolis.

Edited by
Weierstraß-Institut für Angewandte Analysis und Stochastik (WIAS)
Mohrenstraße 39
10117 Berlin
Germany

Fax: + 49 30 2044975
E-Mail: preprint@wias-berlin.de
World Wide Web: http://www.wias-berlin.de/

Abstract

Using a mathematical heat transfer model including anisotropic heat conduction, radiation, and RF heating, we use our software *WIAS-HiTNIHS*[1] to perform numerical computations of the temperature field in axisymmetric growth apparatus during sublimation growth of silicon carbide (SiC) bulk single crystals by physical vapor transport (PVT) (modified Lely method). As it is not unusual for the thermal insulation of PVT growth apparatus to possess an anisotropic thermal conductivity, we numerically study the influence that this anisotropic thermal conductivity has on the temperature field in the growth chamber. Moreover, we also study the influence of the thickness of the insulation. Our results show that, depending on the insulation's orientation, even a moderate anisotropy in the insulation can result in temperature variations of more than 100 K at the growing crystal's surface, which should be taken into account when designing PVT growth apparatus.

1 Introduction

Silicon carbide (SiC) is a wide-bandgap semiconductor used in high-power and high-frequency industrial applications: SiC serves as substrate material for electronic and optoelectronic devices such as MOSFETs, thyristors, blue lasers, and sensors (see [MCB04a] for a recent account of advances in SiC devices). Its chemical and thermal stability make SiC an attractive material to be used in high-temperature applications as well as in intensive-radiation environments. For an economically viable industrial use of SiC, growth techniques for large-diameter, low-defect SiC boules must be available. Recent years have seen steady improvement (see [HBC+04]) of size and quality of SiC single crystals grown by sublimation via *physical vapor transport* (PVT, also known as modified Lely method, see e.g. [Kon95]). However, many problems remain, warranting further research.

Typically, modern PVT growth systems consist of an induction-heated graphite crucible containing polycrystalline SiC source powder and a single-crystalline SiC seed (see Fig. 1). The source powder is placed in the hot zone of the growth apparatus, whereas the seed crystal is cooled by means of a blind hole, establishing a temperature difference between source and seed. As the SiC source is kept at a higher temperature than the cooled SiC seed, sublimation is encouraged at the source and crystallization is encouraged at the seed, causing the partial pressures of Si, Si_2C, and SiC_2 to be higher in the neighborhood of the source and lower in the neighborhood of the seed. As the

[1]**H**igh **T**emperature **N**umerical **I**nduction **H**eating **S**imulator; pronunciation: ~hit-nice.

system tries to equalize the partial pressures, source material is transported to the seed which grows into the reaction chamber.

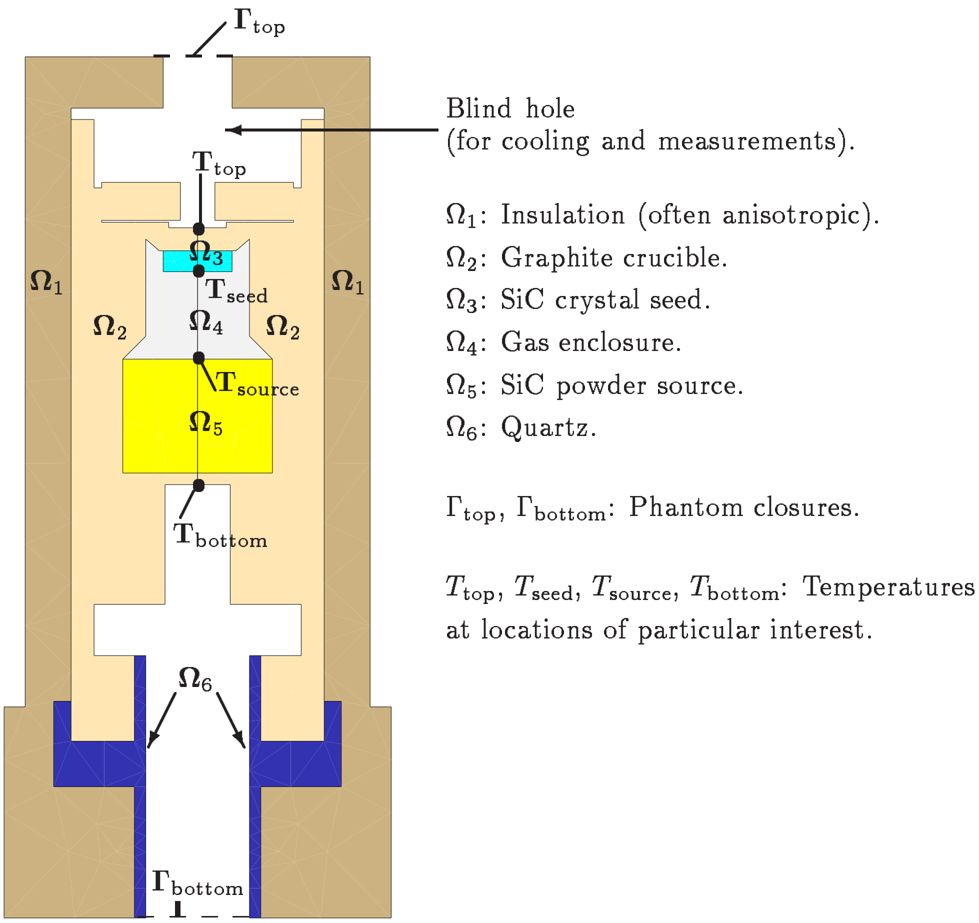

Figure 1: Setup of PVT growth apparatus according to [SSP04, Fig. 4].

Controlling the temperature distribution in the vicinity of SiC seed and source is essential due to its influence on the crystal's quality and growth rate [CZP+01, SSP04]. However, owing to the high temperatures, experimental verification of the correlation between the design of the growth apparatus and the temperature distribution inside the growth chamber is extremely difficult and costly. In consequence, the development of numerical models and software and their application to PVT growth of SiC crystals has been an active field of research in recent years, see, e.g., [KKZ+00, MZPD02, Phi03, KPS04, MPC+04] and references therein.

PVT growth apparatus are usually insulated by graphite felt, where the fibers are aligned in one particular direction, such that the thermal conductivity of the insulation is described by an anisotropic tensor (see Sec. 2 below). The anisotropy factor between the directions parallel and perpendicular to the fibers is usually in the range 1–4 [BSS05].

To the authors' knowledge, the influence of the insulation's anisotropy on the temperature distribution in the growth chamber has not been previously studied in the literature. Our results presented in Sec. 4.2 below show that neglecting the anisotropy of the insulation's thermal conductivity can lead to an error of more than 100 K in the temperature at the crystal seed's surface. The model presented in this article together with its implementation in the software *WIAS-HiTNIHS* thus provides an improved tool in simulation-aided PVT growth apparatus design, especially suitable for tailoring anisotropic thermal insulation.

The paper is organized as follows: In Sec. 2, we describe the mathematical model of the heat transfer, focusing on the description of heat conduction in the presence of materials with anisotropic thermal conductivity. The employed numerical methods and the implementation tools are provided in Sec. 3. Our numerical experiments are presented in Sec. 4, where the general setting is detailed in 4.1, and numerical results showing the influence of anisotropic thermal conductivity in the apparatus insulation, also varying the insulation thickness, are reported on and discussed in 4.2.

2 Modeling of anisotropic heat transfer and induction heating

The numerical results of Sec. 4 below are based on our previously published model of heat transport in induction-heated PVT growth systems (see [Phi03, KPS04] and references therein). The model has been augmented to allow for anisotropic thermal conductivity in the thermal insulation of the growth apparatus as described in the following. In the stationary case, heat conduction in potentially anisotropic materials is described by (see, e.g., [For01]):

$$\operatorname{div} \mathbf{q}_m = f_m, \tag{2.1a}$$

$$\mathbf{q}_m = -K_m(T)\,\nabla T \quad \text{in } \Omega_m, \tag{2.1b}$$

where the index m refers to a material that can be either the gas phase or a solid component of the growth apparatus, $\mathbf{q}_m$ denotes heat flux, f_m denotes power density (per volume) caused in conducting materials due to induction heating, K_m denotes the potentially anisotropic thermal conductivity tensor, T denotes absolute temperature, and Ω_m is the domain of material m.

As described in the Introduction, the PVT growth apparatus is usually insulated by graphite felt, where the fibers are aligned in one particular direction, resulting in a bias towards heat transport parallel to the fibers as compared with the perpendicular direction. Assuming that the fiber alignment and the resulting anisotropy do not vary with the temperature, the thermal conductivity tensor is a diagonal matrix of the following form:

$$K_m(T) = \big(\kappa^m_{i,j}(T)\big), \quad \text{where} \quad \kappa^m_{i,j}(T) = \begin{cases} \alpha^m_i\, \kappa^m_{\text{iso}}(T) & \text{for } i = j, \\ 0 & \text{for } i \neq j, \end{cases} \tag{2.2}$$

$\kappa^m_{\text{iso}}(T)$ being the potentially temperature-dependent thermal conductivity of the isotropic case, and α^m_i being anisotropy coefficients.

Apart from the modified, potentially anisotropic heat flux $\mathbf{q}_m$ according to (2.1b) and (2.2), all interface and boundary conditions are exactly as described in [KPS04, Sec. 2.4]. In particular, the temperature is assumed to be continuous throughout the apparatus, and radiative heat transfer between surfaces of cavities is modeled using the net radiation method for diffuse-gray radiation as described in [KPS04, Sec. 2.5], where a band approximation model is used to account for the semi-transparency of the SiC single crystal. The growth apparatus is considered in a black body environment (e.g. a large isothermal room) radiating at room temperature T_{room}, such that outer boundaries emit according to the Stefan-Boltzmann law. For the two blind holes, we use black body phantom closures (denoted by Γ_{top} and Γ_{bottom} in Fig. 1) which emit radiation at T_{room}. We thereby allow for radiative interactions between the open cavities and the ambient environment, including reflections at the cavity surfaces.

Induction heating causes eddy currents in the conducting materials of the growth apparatus, resulting in the heat sources f_m of (2.1a) due to the Joule effect. Assuming axisymmetry of all components of the growth system as well as of all relevant physical quantities, and, furthermore, assuming sinusoidal time dependence of the imposed alternating voltage, the heat sources are computed via an axisymmetric complex-valued magnetic scalar potential that is determined as the solution of an elliptic partial differential equation (see [KPS04, Sec. 2.6]). To prescribe the total heating power, we follow [KP02, Sec. II], ensuring that the total current is the same in each coil ring.

All simulations presented in this article are performed for an idealized growth apparatus, treating all solid materials as homogeneous and pure, neglecting effects such as the sintering of the SiC source powder, changes in the porosity of the graphite, and Si accumulation in the insulation. Furthermore, it is assumed that the gas phase is made up solely of argon, which is a reasonable assumption for simulations of the temperature distribution [KPSW01, Sec. 5].

3 Numerical methods and implementation

For the numerical computations presented in Sec. 4 below, the nonlinear partial differential equations arising from the mathematical heat transfer model described in Sec. 2 above are discretized using the finite volume method. The used scheme, including the discretization of nonlocal terms stemming from the modeling of diffuse-gray radiation, was previously described in [Phi03, KP05]; modifications to allow for the anisotropic thermal conductivity are treated in [GKP05]. Also in [GKP05], for some simple anisotropic test cases, we verified the accuracy of our finite volume scheme, comparing the numerical results with known exact solutions and determining the numerical convergence rate.

The finite volume discretization of the nonlocal radiation terms involves the calculation of visibility and view factors. The method used is based on [DNR⁺90] and is described in [KPSW01, Sec. 4].

The discrete scheme was implemented as part of our software *WIAS-HiTNIHS* which is based on the program package *pdelib* [FKL01]. In particular, *pdelib* uses the grid generator *Triangle* [She96] to produce constrained Delaunay triangulations of the domains, and it uses the sparse matrix solver *PARDISO* [SGF00, SG04] to solve the linear system arising from the linearization of the finite volume scheme via Newton's method.

4 Numerical experiments

4.1 General setting

All numerical simulations presented in the following were performed for a growth apparatus shaped according to [SSP04, Fig. 4], which is displayed in Fig. 1. For radius and height of this apparatus, we use 10.1 cm and 45.3 cm, respectively. Moreover, we place this apparatus inside 5 hollow, rectangular-shaped copper induction rings, where the coil's lower and upper rim are at 19.5 cm and 40 cm, respectively. The geometric proportions of the coil rings are provided in Fig. 2.

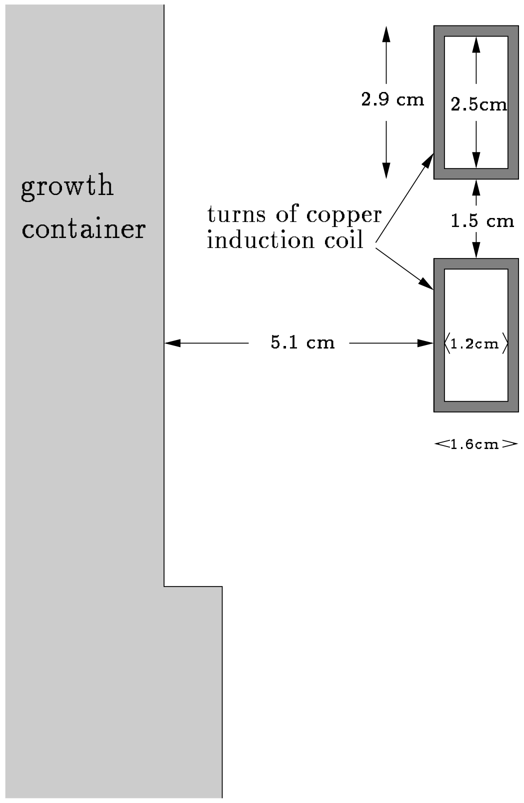

Figure 2: Geometric proportions of induction coil rings.

As shown in Fig. 1, the considered apparatus consists of six materials: insulation, graphite crucible, SiC crystal seed, gas enclosure, SiC powder source, and quartz. Except for the insulation and for quartz, the material data used for the above materials during the following numerical experiments are precisely the data provided in the appendices of [KPSW01] and [KP03], respectively. The material data we use for the insulation are also provided in [KPSW01, App. 2.2], except that, here, we use anisotropic thermal conductivities as described below. The material data we use for quartz are provided in Appendix A below. In particular, for the isotropic parts $\kappa^m_{\text{iso}}(T)$ of the thermal conductivity tensors (cf. (2.2)), for gas enclosure, graphite crucible, insulation, and SiC crystal seed, we use the functions given by (A.1), (A.3b), (A.4b), and (A.7b) in [KPSW01], respectively; for $\kappa^5_{\text{iso}}(T)$ (SiC powder source), we use [KP03, (A.1)], and for $\kappa^6_{\text{iso}}(T)$ (quartz), we use (A.1c) from Appendix A below.

As mentioned in the Introduction and in Sec. 2 above, the thermal conductivity in the insulation of PVT growth apparatus is typically anisotropic and has the form (2.2). In Sec. 4.2 below, we will assess the influence of the insulation's anisotropic thermal conductivity on the temperature field in the growth apparatus. To this end, in the numerical experiments reported on in Sec. 4.2, we vary the anisotropy coefficients (α^1_r, α^1_z) of the insulation while keeping $(\alpha^m_r, \alpha^m_z) = (1, 1)$ for all other materials $m \in \{2, \dots, 5\}$.

The angular frequency used for the induction heating is $\omega = 2\pi f$, where $f = 10$ kHz. The prescribed average total power is $P = 10$ kW.

4.2 Numerical results

Within the general setting described in the previous section, we conduct two series of numerical experiments. In the first series, the growth apparatus is exactly as in Fig. 1 with the dimensions as specified in the previous section. In the second series, we study the influence of increasing the thickness of the insulation, as this is a possibility to compensate for additional heat loss caused by the anisotropic thermal conductivity. We consider the details of the second series after the following discussion of the first series.

The first series consists of five numerical simulations, varying the anisotropy coefficients (α^1_r, α^1_z) in the insulation. The five numerical experiments will be referred to as experiments (a) – (e). In experiment (a), we consider the isotropic case, i.e. $(\alpha^1_r, \alpha^1_z) = (1, 1)$ throughout Ω_1. Experiments (b) and (c) use $(\alpha^1_r, \alpha^1_z) = (4, 1)$ and $(\alpha^1_r, \alpha^1_z) = (1, 4)$ throughout Ω_1, respectively. As mentioned in the Introduction, such anisotropy factors are found in physical growth experiments [BSS05]. In a reasonable apparatus design, one would try to take advantage of the insulation's anisotropy, using different orientations of the insulation material for different parts of the apparatus (e.g. one orientation for the side walls and a different orientation for top and bottom). To assess the impact of using such different orientations for the insulation, for the two remaining numerical experiments (d) and (e), we divide the insulation region Ω_1 of Fig. 1 into five subregions, denoted by numbers $1, \dots, 5$ in Figures 3 – 7. In experiment (d), we set $(\alpha^1_r, \alpha^1_z) = (4, 1)$ in insulation regions 1, 5, and $(\alpha^1_r, \alpha^1_z) = (1, 4)$ in insulation regions 2, 3, 4. In experiment (e), we set $(\alpha^1_r, \alpha^1_z) = (4, 1)$ in insulation regions 1, 2, 4, 5, and $(\alpha^1_r, \alpha^1_z) = (1, 4)$ in insulation region 3. The settings of the (α^1_r, α^1_z) during the experiments of the first series are compiled in Table 1 together with computed temperature values and with references to figures depicting the computed temperature fields.

Exp.	Figure	Ins. regions	(α_r^1, α_z^1)	$T_{\rm max}$ $[K]$	$T_{\rm top}$ $[K]$	$T_{\rm bottom}$ $[K]$	$T_{\rm seed}$ $[K]$	$T_{\rm source}$ $[K]$
(a)	3, right	1,2,3,4,5	$(1,1)$	2552.46	2433.35	2199.65	2497.48	2523.53
(b)	4, left	1,2,3,4,5	$(4,1)$	1835.39	1800.1	1599.3	1815.71	1828.74
(c)	4, right	1,2,3,4,5	$(1,4)$	2458.72	2312.67	2148.59	2380.57	2416.46
(d)	5, right	1,5 2,3,4	$(4,1)$ $(1,4)$	2522.80	2401.21	2183.3	2464.89	2492.48
(e)	5, left	1,2,4,5 3	$(4,1)$ $(1,4)$	2515.55	2393.51	2171.62	2457.21	2485.11

Table 1: Computed temperature values for first series of numerical experiments, varying the anisotropy coefficients (α_r^1, α_z^1) in the insulation regions $1, \dots, 5$ (maximal temperature $T_{\rm max}$ and temperatures at points of particular interest (see Fig. 1)).

In Figure 3, we show the computed heat source field (left) as well as the computed temperature field (right) for experiment (a), i.e. for the isotropic case. Due to the well-known moderate skin effect occurring during RF heating, the heat sources are concentrated close to the surface of the graphite crucible. The depicted temperature field shows that the maximal temperature is established close to the surface of the powder source. Together with the cooling effect of the upper blind hole, this results in the necessary temperature difference being present between SiC source and crystal seed.

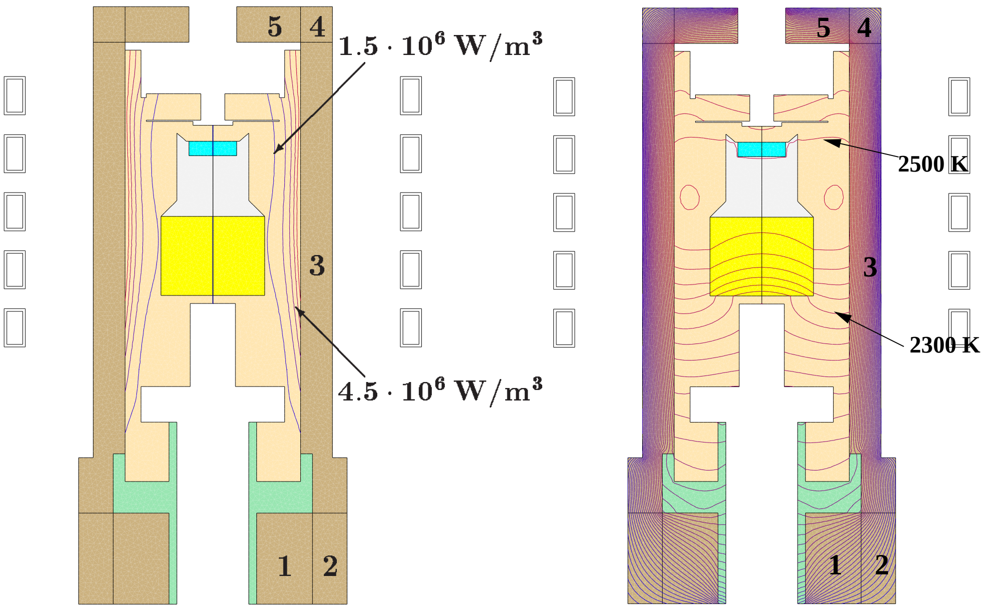

Figure 3: Heat source field (left) and temperature field (right) computed for experiment (a) of first series of experiments, i.e. for an isotropic insulation $(\alpha_r^1, \alpha_z^1) = (1,1)$ (cf. Table 1). In the heat source field, the isolines are spaced at $1.5 \cdot 10^6$ W/m^3; in the temperature field, the isotherms are spaced at 50 K.

Figures 4 and 5 show the computed temperature fields for the anisotropic cases (b)

– (e) of the first series. Comparing each of these temperature fields to the result of the isotropic case (Fig. 3) shows that the overall temperature is lower in all of the anisotropic cases. This is also seen in each of the particular temperatures tracked in Table 1. The lower temperatures are expected, since setting either $\alpha_r^1 = 4$ or $\alpha_z^1 = 4$ in any of the insulation regions results in improving that region's thermal conductivity by a factor of four in either the radial or the vertical direction. Thus, the thermal insulation becomes less effective, resulting in a lower overall temperature. This effect is especially dramatic in experiment (b), where $\alpha_r^1 = 4$ throughout the insulation. Here, originating from the heat sources in the outer region of the graphite susceptor, the heat is radially transported to the outer side wall and radiated off, reducing the temperature in the growth chamber by almost 600 K. When constructing the growth apparatus, one would therefore always want to orient the insulation at the side wall (region 3) such that the preferred direction of thermal conductivity is in the vertical direction as in experiments (c) – (e). The right picture in Fig. 4 as well as Table 1 show that in case (c) ($\alpha_z^1 = 4$ throughout insulation), the temperature T_{seed} at the surface of the seed crystal is still more than 100 K lower than in the isotropic case (a). However, one can once again improve the insulation's effectiveness by radially orienting the preferred direction of heat transport in the top and bottom regions 5 and 1 (experiments (d) and (e), see Fig. 5 and Table 1). In these cases, T_{seed} is merely 30 – 40 K lower than in the isotropic case (a). The orientation of the corner pieces 2 and 4 has only a small effect with a slightly improved insulation in case (d) (i.e. $(\alpha_r^1, \alpha_z^1) = (1, 4)$ in 2, 4) as compared to case (e). Thus, according to our results, (d) this is the design we recommend for the construction of PVT growth apparatus.

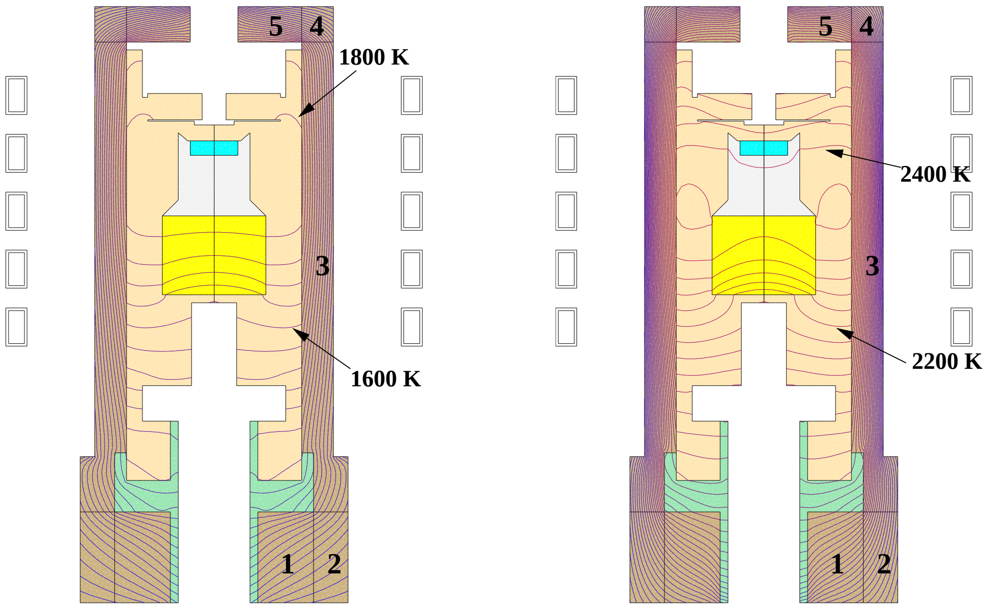

Figure 4: Computed temperature fields for experiments (b) (left) and (c) (right) of first series of experiments, i.e. for anisotropic insulations with $(\alpha_r^1, \alpha_z^1) = (4, 1)$ (left) and $(\alpha_r^1, \alpha_z^1) = (1, 4)$ (right) (cf. Table 1). The isotherms in both pictures are spaced at 50 K.

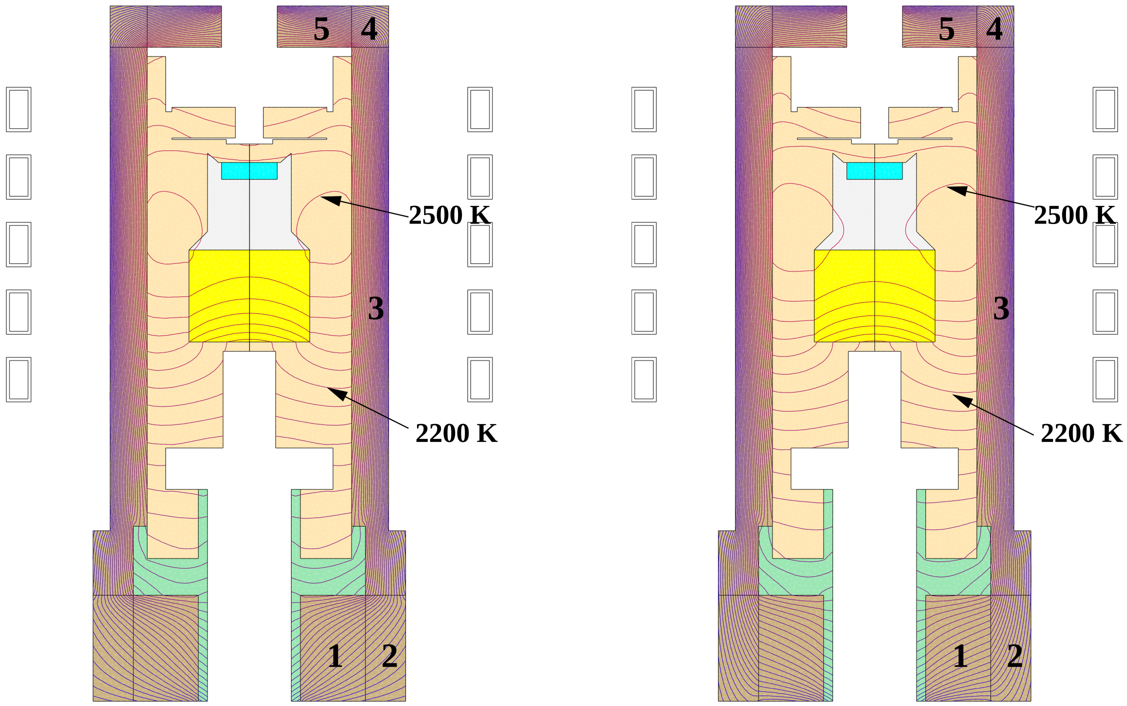

Figure 5: Computed temperature fields for experiments (e) (left) and (d) (right) of first series of experiments, i.e. for anisotropic insulations with $(\alpha_r^1, \alpha_z^1) = (4, 1)$ in regions 1, 2, 4, 5 and $(\alpha_r^1, \alpha_z^1) = (1, 4)$ in region 3 (left); and with $(\alpha_r^1, \alpha_z^1) = (4, 1)$ in regions 1, 5 and $(\alpha_r^1, \alpha_z^1) = (1, 4)$ in regions 2, 3, 4 (right) (cf. Table 1). The isotherms in both pictures are spaced at 50 K.

Another important observation when comparing Figures 3 – 5 is the stability of the qualitative form of the temperature field in the inner growth apparatus: While the absolute level of the temperature is noticeably reduced in the anisotropic cases (b) – (e), the shapes and distances of the isotherms are very similar in cases (a) and (c) – (e), the temperature field merely being shifted to the lower temperature level (in case (b), the temperature reduction is sufficiently large to flatten the isotherms near the axis). The qualitative similarity of the isotropic and anisotropic temperature fields is particularly clear in the close-ups shown in Fig. 6, comparing the temperature fields in the seed crystal's vicinity for the isotropic case (a) and the anisotropic case (e).

Summarizing the results of the first series of experiments, it is important to account for an anisotropic thermal conductivity when calculating the temperature field in PVT growth systems, since, even for realistic anisotropies of factor four, temperature changes can be significant in the growth chamber. Choosing the orientation of the insulation wisely can minimize the anisotropy-related heat loss. Even in experiment (d), showing the smallest differences when compared with the isotropic case (a), the temperature at the seed crystal's surface is reduced by some 35 K, which can be significant when fine-tuning the temperature field, e.g. to ensure the growth of a particular SiC polytype. On the other hand, the anisotropy-related heat loss mainly shifts the temperature field of the inner growth apparatus to a lower overall temperature, leaving its overall shape

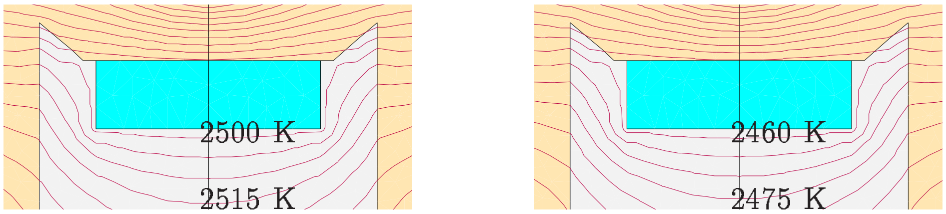

Figure 6: Close-ups showing the computed temperature fields in the vicinity of the SiC seed crystal for experiments (a) (left) and (e) (right) of first series of experiments, i.e. for an isotropic insulation $(\alpha_r^1, \alpha_z^1) = (1, 1)$ in regions $1 - 5$ (left); and for an anisotropic insulation with $(\alpha_r^1, \alpha_z^1) = (4, 1)$ in regions 1, 2, 4, 5 and $(\alpha_r^1, \alpha_z^1) = (1, 4)$ in region 3 (right) (cf. Table 2). The isotherms in both pictures are spaced at 5 K.

almost unaffected. In particular, the temperature gradients between crystal source and seed do not depend significantly on the insulation's thermal anisotropy.

In the thermally anisotropic insulation, whenever α_r^1 or α_z^1 is larger than 1, the heat is conducted faster in the corresponding direction. Thus, more heat is radiated off into the ambient environment, resulting in the above-discussed reduced overall temperature in the growth chamber. The idea is now to compensate for this effect by using a thicker insulation, which is the case considered in our second series of numerical experiments.

Increasing the thickness of the thermal insulation of the growth apparatus is the only difference to the first series of numerical experiments. For the second series, 3 cm of insulation were added at the side wall and 5 cm of insulation were added at the top of the apparatus such that the new apparatus has a radius of 13.1 cm and a height of 50.3 cm. The geometric proportions of the coil rings are still as specified in Fig. 2, but now with respect to the new apparatus.

As did the first series, the second series also consists of five numerical experiments denoted by (a) – (e), varying the anisotropy coefficients (α_r^1, α_z^1) in the insulation. As in the first series, we choose $(\alpha_r^1, \alpha_z^1) = (1, 1)$ throughout Ω_1 for (a) (isotropic case); $(\alpha_r^1, \alpha_z^1) = (4, 1)$ throughout Ω_1 for (b); $(\alpha_r^1, \alpha_z^1) = (1, 4)$ throughout Ω_1 for (c); $(\alpha_r^1, \alpha_z^1) = (4, 1)$ in insulation regions 1, 5, and $(\alpha_r^1, \alpha_z^1) = (1, 4)$ in insulation regions 2, 3, 4 for (d); $(\alpha_r^1, \alpha_z^1) = (4, 1)$ in insulation regions 1, 2, 4, 5, and $(\alpha_r^1, \alpha_z^1) = (1, 4)$ in insulation region 3 for (e). The settings of the (α_r^1, α_z^1) during the experiments of the second series are compiled in Table 2 together with computed temperature values and, where applicable, with references to figures depicting the computed temperature fields.

In Figure 7, we present the computed temperature fields for experiments (a) and (e) of the second series. Comparing the isotropic cases (a) of both series (see Fig. 7 (left), Fig. 3 (right) and cases (a) in Tables 1, 2), the temperature at the seed crystal's surface T_{seed} is raised by almost 300 K due to the thicker insulation. The temperature difference between source and seed is reduced, as radiative heat transfer becomes more effective in the growth chamber (cf. [KPSW01]). Moreover, the thicker insulation leads to larger temperature differences between the isotropic case (a) and the anisotropic cases (b)

Exp.	Figure	Ins. regions	(α_r^1, α_z^1)	T_{max} $[K]$	T_{top} $[K]$	T_{bottom} $[K]$	T_{seed} $[K]$	T_{source} $[K]$
(a)	7, left	1,2,3,4,5	$(1,1)$	2813.23	2711.15	2406.76	2773.97	2789.8
(b)		1,2,3,4,5	$(4,1)$	2001.92	1970.49	1761.28	1986.69	1995.66
(c)		1,2,3,4,5	$(1,4)$	2678.27	2563.32	2331.39	2627	2648.88
(d)		1,5 2,3,4	$(4,1)$ $(1,4)$	2745.01	2642.8	2375.33	2703.82	2721.32
(e)	7, right	1,2,4,5 3	$(4,1)$ $(1,4)$	2719.13	2609.78	2358.83	2673.7	2693.34

Table 2: Computed temperature values for second series of numerical experiments (thicker insulation), varying the anisotropy coefficients (α_r^1, α_z^1) in the insulation regions $1, \ldots, 5$ (maximal temperature T_{max} and temperatures at points of particular interest (see Fig. 1)).

– (e) (compare Tables 1 and 2), making it even more important to account for the anisotropic thermal conductivity to compute accurate temperature fields. Otherwise, the calculations of the second series confirm the results of the first series: Orienting the insulation differently in the regions 1 – 5 according to case (d) results in the smallest temperature difference as compared with the isotropic case (a) (however, here the difference in T_{seed} is still some 70 K (Table 2), about twice as much as for the thinner insulation). As for the thinner insulation, the temperature fields in the inner growth apparatus are qualitatively very similar in the isotropic and anisotropic cases (with the exception of case (b)). For the cases (a) and (e), this can be seen in Fig. 7.

Summarizing these phenomena, thickening the insulation results in higher temperatures in the growth apparatus and leads to more prominent differences between the isotropic and the anisotropic situation (cf. abovedescribed decrease for T_{seed}). Thickening the insulation can be used to partially compensate for the effect of the insulation's anisotropic thermal conductivity. In any case, an optimal insulation design needs to take an anisotropic thermal conductivity into account.

5 Conclusions

Based on a model describing the heat transfer in PVT growth systems, including RF heating, heat conduction allowing for anisotropic thermal conductivity tensors, and radiation between cavity surfaces, we used our simulation software *WIAS-HiTNIHS* to conduct numerical investigations of the temperature field established in PVT growth apparatus. Using realistic values of anisotropy coefficients, it was shown that neglecting the anisotropy of the thermal conductivity in the apparatus insulation, can lead to significant errors, when calculating the temperature field in the growth chamber. For a fixed heating power, the temperature differences between the isotropic and anisotropic cases can reach several hundred Kelvin, depending on the orientation of the thermal insulation. Even for an optimized orientation of the insulation, the temperature dif-

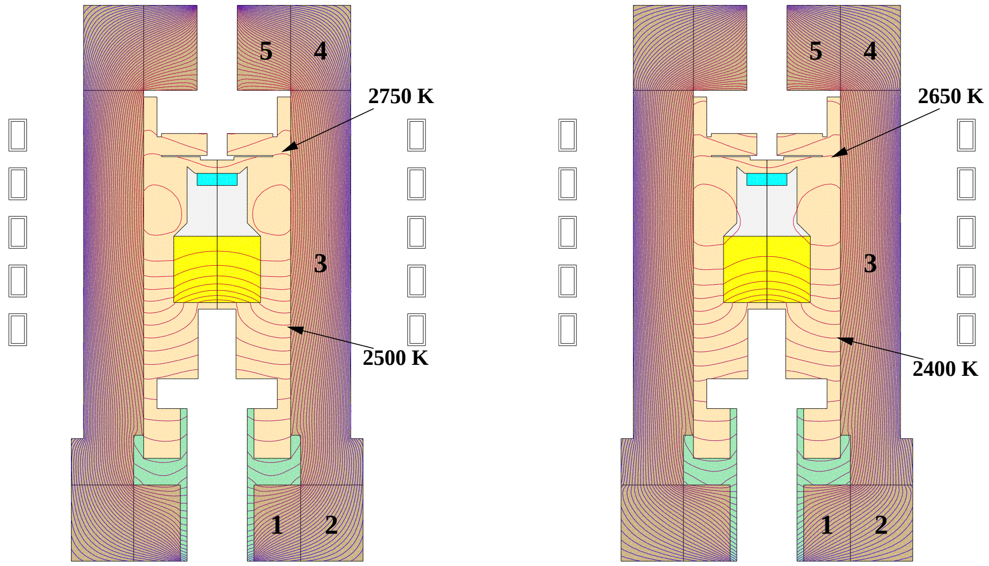

Figure 7: Computed temperature fields for experiments (a) (left) and (e) (right) of second series of experiments, i.e. for an isotropic insulation $(\alpha_r^1, \alpha_z^1) = (1, 1)$ in regions $1-5$ (left); and for an anisotropic insulation with $(\alpha_r^1, \alpha_z^1) = (4, 1)$ in regions 1, 2, 4, 5 and $(\alpha_r^1, \alpha_z^1) = (1, 4)$ in region 3 (right) (cf. Table 2). The isotherms in both pictures are spaced at 50 K.

ference at the seed crystal's surface was still between 35 and 70 K, depending on the insulation's thickness. This difference can be sufficiently large to result in the growth of unwanted SiC polytypes. Thickening the insulation can be used to partially compensate for the effect of the insulation's anisotropic thermal conductivity. The qualitative form of the temperature field in the growth chamber and, thus, the temperature gradients between SiC source and seed were not significantly affected by the insulation's thermal anisotropy. In particular, the presented results show that the software tool *WIAS-HiTNIHS*, augmented by the presented capability to account for materials with anisotropic thermal conductivities, constitutes an improved tool for computer-aided PVT growth system optimization.

6 Acknowledgments

We thank Jürgen Sprekels (WIAS Berlin), Klaus Böttcher, Detlev Schulz, and Dietmar Siche (all IKZ Berlin) for helpful discussions and advice.

A Appendix: Material data for quartz

The material parameters used for electrical conductivity $\sigma_c^{\mathrm{quartz}}$, mass density ρ^{quartz}, isotropic thermal conductivity $\kappa_{\mathrm{iso}}^{\mathrm{quartz}}$, and emissivity $\epsilon^{\mathrm{quartz}}$ of quartz are

$$\sigma_c^{\mathrm{quartz}}(T) = 0, \tag{A.1a}$$

$$\rho^{\mathrm{quartz}}(T) = 2600\,\frac{\mathrm{kg}}{\mathrm{m}^3}, \tag{A.1b}$$

$$\kappa_{\mathrm{iso}}^{\mathrm{quartz}}(T) = \left(1.82 - 1.21\cdot 10^{-3}\,\frac{T}{\mathrm{K}} + 1.75\cdot 10^{-6}\,\frac{T^2}{\mathrm{K}^2}\right)\frac{\mathrm{W}}{\mathrm{m\,K}}, \tag{A.1c}$$

$$\epsilon^{\mathrm{quartz}}(T) = 0.82 + 3.50\cdot 10^{-5}\,\frac{T}{\mathrm{K}}. \tag{A.1d}$$

References

[BSS05] K. Böttcher, D. Schulz, and D. Siche. Institute for Crystal Growth (IKZ), Berlin, 2005, private communication.

[CZP+01] Q.-S. Chen, H. Zhang, V. Prasad, C.M. Balkas, and N.K. Yushin. *Modeling of heat transfer and kinetics of physical vapor transport growth of silicon carbide crystals.* Transactions of the ASME. Journal of Heat Transfer **123** (2001), No. 6, 1098–1109.

[DNR+90] F. Dupret, P. Nicodéme, Y. Ryckmans, P. Wouters, and M.J. Crochet. *Global modelling of heat transfer in crystal growth furnaces.* Intern. J. Heat Mass Transfer **33** (1990), No. 9, 1849–1871.

[FKL01] J. Fuhrmann, Th. Koprucki, and H. Langmach. *pdelib: An open modular tool box for the numerical solution of partial differential equations. Design patterns*, in [HW01].

[For01] V.F. Formalev. *Heat and Mass Transfer in Anisotropic Bodies.* High Temperature **39** (2001), No. 5, 753–774.

[GKP05] J. Geiser, O. Klein, and P. Philip. *Numerical simulation of heat transfer in materials with anisotropic thermal conductivity: A finite volume scheme to handle complex geometries.* Preprint No. ???, Weierstraß-Institut für Angewandte Analysis und Stochastik, Berlin, 2005.

[Har95] G.L. Harris (ed.). *Properties of Silicon Carbide.* EMIS Datareview Series, no. 13, Institution of Electrical Engineers, INSPEC, London, UK, 1995.

[HBC+04] H.McD. Hobgood, M.F. Brady, M.R. Calus, J.R. Jenny, R.T. Leonard, D.P. Malta, St.G. Müller, A.R. Powell, V.F. Tsvetkov, R.C. Glass, and C.H. Carter, Jr. *Silicon Carbide Crystal and Substrate Technology: A Survey of Recent Advances.* Mater. Sci. Forum

457–**460** (2004), 3–8, Proceedings of the 10th International Conference on Silicon Carbide and Related Materials, October 5–10, 2003, Lyon, France.

[HW01] W. Hackbusch and G. Wittum (eds.). *Proceedings of the 14th GAMM Seminar on Concepts of Numerical Software, Kiel, January 23–25, 1998.* Kiel, Germany, University of Kiel, 2001.

[KKZ+00] S.Yu. Karpov, A.V. Kulik, I.A. Zhmakin, Yu.N. Makarov, E.N. Mokhov, M.G. Ramm, M.S. Ramm, A.D. Roenkov, and Yu.A. Vodakov. *Analysis of sublimation growth of bulk SiC crystals in tantalum container.* J. Crystal Growth **211** (2000), 347–351.

[Kon95] A.O. Konstantinov. *Sublimation growth of SiC*, in [Har95], pp. 170–203.

[KP02] O. Klein and P. Philip. *Correct voltage distribution for axisymmetric sinusoidal modeling of induction heating with prescribed current, voltage, or power.* IEEE Trans. Mag. **38** (2002), No. 3, 1519–1523.

[KP03] O. Klein and P. Philip. *Transient temperature phenomena during sublimation growth of silicon carbide single crystals.* J. Crystal Growth **249** (2003), No. 3–4, 514–522.

[KP05] O. Klein and P. Philip. *Transient Conductive-Radiative Heat Transfer: Discrete Existence and Uniqueness for a Finite Volume Scheme.* Math. Mod. Meth. Appl. Sci. **15** (2005), No. 2, 227–258.

[KPS04] O. Klein, P. Philip, and J. Sprekels. *Modeling and simulation of sublimation growth of SiC bulk single crystals.* Interfaces and Free Boundaries **6** (2004), 295–314.

[KPSW01] O. Klein, P. Philip, J. Sprekels, and K. Wilmański. *Radiation- and convection-driven transient heat transfer during sublimation growth of silicon carbide single crystals.* J. Crystal Growth **222** (2001), No. 4, 832–851.

[MCB04a] Ch. 9–11 in Madar et al. [MCB04b], 2004.

[MCB04b] Roland Madar, Jean Camassel, and Elisabeth Blanquet (eds.). *Silicon Carbide and Related Materials ICSCRM, Lyon, France, October 5–10, 2003.* Materials Science Forum, Vol. 457–460, Part II, Trans Tech Publications Ltd, 2004.

[MPC+04] J. Meziere, M. Pons, L. Di Cioccio, E. Blanquet, P. Ferret, J.M. Dedulle, F. Baillet, E. Pernot, M. Anikin, R. Madar, and T. Billon. *Contribution of numerical simulation to silicon carbide bulk growth and epitaxy.* J. Phys.-Condes. Matter **16** (2004), S1579–S1595.

[MZPD02] R. Ma, H. Zhang, V. Prasad, and M. Dudley. *Growth Kinetics and Thermal Stress in the Sublimation Growth of Silicon Carbide.* Crystal Growth & Design **2** (2002), No. 3, 213–220.

[Phi03] P. Philip. *Transient Numerical Simulation of Sublimation Growth of SiC Bulk Single Crystals. Modeling, Finite Volume Method, Results.* Ph.D. thesis, Department of Mathematics, Humboldt University of Berlin, Germany, 2003, Report No. 22, Weierstraß-Institut für Angewandte Analysis und Stochastik, Berlin.

[pro96] *First Workshop on Applied Computational Geometry (Philadelphia, Pennsylvania).* ACM, May 1996.

[SG04] O. Schenk and K. Gärtner. *Solving Unsymmetric Sparse Systems of Linear Equations with PARDISO.* Journal of Future Generation Computer Systems **20** (2004), No. 3, 475–487.

[SGF00] O. Schenk, K. Gärtner, and W. Fichtner. *Scalable Parallel Sparse Factorization with Left-Strategy on Shared Memory Multiprocessor.* BIT **40** (2000), No. 1, 158–176.

[She96] J.R. Shewchuk. *Triangle: Engineering a 2D Quality Mesh Generator and Delaunay Triangulator*, in [pro96], pp. 124–133.

[SSP04] K. Semmelroth, N. Schulze, and G. Pensl. *Growth of SiC polytypes by the physical vapour transport technique.* J. Phys.-Condes. Matter **16** (2004), S1597–S1610.